Eur. Phys. J. Appl. Phys. (2014) 65: 10201
DOI: 10.1051/epjap/2013130517

THE EUROPEAN PHYSICAL JOURNAL APPLIED PHYSICS

Regular Article

Enhanced photovoltaic conversion efficiency in bulk heterojunction solar cells upon incorporating nanohybridized PbS quantum dots/multiwall carbon nanotubes

Jayanta Kumar Baral[1,2,3,a], Ankit Sharma[2], Defa Wang[4], Dongling Ma[4], Vo-Van Truong[3], and Ricardo Izquierdo[2]

[1] Department of Polymer Science and Engineering, University of Massachusetts (UMass), Amherst, 120 Governors Drive, Massachusetts 01003, United States of America
[2] NanoQAM, Département d'informatique, University of Quebec at Montreal (UQAM), Case postale 8888, succursale Centre-ville, Montreal, Quebec H3C 3P8, Canada
[3] Department of Physics, Concordia University, 7141 Sherbrooke (West), Montreal, Quebec H4B 1R6, Canada
[4] Institut National de la Recherche Scientifique, INRS-Énergie, Matériaux et Télécommunications, 1650 Boulevard Lionel-Boulet, Varennes, Quebec J3X 1S2, Canada

Received: 13 November 2013 / Received in final form: 11 December 2013 / Accepted: 12 December 2013
Published online: 17 January 2014 –

Abstract. We report on a modified bulk heterojunction (BHJ) solar cell in which a nanohybridized composition of lead sulfide (PbS) colloidal quantum dots (QDs) and multiwall carbon nanotubes (MWCNTs) were incorporated into a standard regioregular poly(3-hexylthiophene) (rr-P3HT):phenyl-C_{61}-butyric acid methyl ester (PCBM) blend. This hybrid ((P3HT:PCBM):PbS-QD/MWCNT) solar cell exhibits an increased power conversion efficiency (PCE) of 3.40% as compared to that of 2.57% from a controlled P3HT:PCBM standard BHJ solar cell fabricated under similar experimental conditions. The 32% increase in efficiency is effectively attributed to the extended quantum-dot-sensitization in the near-infrared (NIR) due to the absorbance of QDs/CNTs in the spectral range from 700 nm to 1450 nm. The strong conjugation, controlled coupling and nanohybridization of QDs/CNTs played an important role towards the improvement of PCE since it is proposed that excitons generated in the QDs can be efficiently dissociated at the QD/CNT interface by transferring the electrons to the CNTs followed by holes transfer to the P3HT. In this ternary blend, the staggered energy band alignment between P3HT and the QDs allows both electrons and holes transfer from the QDs to the PCBM and the P3HT, respectively. Subsequently, the dissociated carriers have been efficiently transported by the CNTs and P3HT to favorable respective electrodes.

1 Introduction

Polymer solar cells are emerging as the alternative inexpensive renewable source of green energy due to their interesting properties, such as, low-temperature based manufacturing, mechanical flexibility and solution processability [1–12]. Recently, the power conversion efficiency (PCE) of OPV devices has exceeded the 10% milestone [11,12]. However, this performance is still not optimal for commercial viability. One of the most commonly used materials in polymer solar cells is a blend of polymer/fullerene (in particularly, the nanocomposite of poly(3-hexylthiophene):phenyl-C_{61}-butyric acid methyl ester (in short, P3HT:PCBM) [13]. One of the limiting factors that hinder the performance of these organic photovoltaic cells is the negligible absorption in near-infrared (NIR) and/or infrared (IR) of the solar spectrum.

However, the spectral sensitivity of the solar cells can be extended beyond the visible range by using blends of different materials. By this approach, the photodiodes exhibited the increase in photo-current without any significant loss of voltage [14]. This can potentially be achieved by using colloidal nanocrystal quantum dots (QDs) as the light-harvesting materials since their optical band gap can be fine-tuned to the desired range by choosing the appropriate material composition and by controlling nanocrystal size during synthesis [15–17]. Among the QD materials, the lead sulfide (PbS) – and lead selenide (PbSe) – QDs possess excellent spectral-photo-sensitivity for the near-infrared absorption of the spectrum [18]. Moreover, the PbS-QDs are capable of generating multiple

[a] e-mail: jkbaral@gmail.com

excitons [19,20]. The performance, in terms of PCE, of these QD based PV cells have been reached up to ∼2.0% under one sun AM1.5 test conditions as reported [21–24]. Upon incorporating the PbS-QDs into the solution processable polymer PV cells, the short-circuit current density (J_{sc}) was significantly increased without losing open-circuit voltage (V_{oc}) and as a result the efficiency was also improved by two-folds [25]. However, the PbS-QDs alone cannot contribute significantly well to the PV performances, since these PbS-QDs formed mid-gap recombination, deep traps and consequent catastrophic loss of the performance [18]. The charge transport is effectively hampered due to the mid-gap recombination and deep career trapping, hence the modest performance observed from these QD based PV cells. The charge transport can effectively be improved upon incorporating the carbon nanotubes (CNTs) into the photoactive layer of polymer PV cells. As a result, the power conversion efficiency could significantly enhanced due to the improved carrier transport through ballistic pathways provided by CNTs instead of slow hopping and tunneling among phase separated clusters [26–30].

In one of our previous communication [31], where we have reported a hybrid photoactive layer prepared from a modified blend of P3HT (without PCBM) and nanohybridized PbS/MWCNT, in place of standard P3HT:PCBM. The P3HT:PbS/MWCNT solar cell shown an improved PCE enhancement while PCBM was replaced by nanohybridized PbS/MWCNT. In this current work, we propose an alternative approach for introducing such organic/inorganic nanohybridized composites into the photoactive layers of the standard BHJ polymer solar cells. We start by synthesizing nanohybrids of PbS/MWCNT, with strong conjugation, and controlled coupling of the PbS-QDs in the close proximity to the MWCNTs. Herein, we used the nano-engineered composite of lead sulfide quantum dot (QD) and multiwall carbon nanotube (MWCNT) in order to achieve a higher degree of charge dissociation, separation and transfer efficiency. Those controlled coupling and nanohybridized QDs/CNTs composites were then further incorporated into the standard photoactive blend of polymer/fullerene. The PbS-QDs were attached, by hydrophobic reactions, onto the surfaces of MWCNTs which were employed in order to facilitate the electron transport to the collecting electrode(s). This approach can significantly extend the wavelength absorption of the polymer solar cell in the near-infrared (NIR) ranging from 700 nm to 1450 nm and at the same time preserve the charge transport and collection of generated carriers that result in an improvement in PCE.

2 Experimental details and device fabrication

2.1 Chemical synthesis of PbS-QDs by using OLA as ligands

PbS QDs were synthesized by an organometallic chemistry method using OLA as ligands [31,32]. Typically, $PbCl_2$ (278 mg, 1 mMol, Sigma-Aldrich) and OLA (5 mL, Sigma-Aldrich, technical grade, 70%) were loaded into a 50 mL three-neck flask at room temperature. The mixture was first purged by N_2 gas for 45 min to remove oxygen and then heated to 90 °C to form the homogeneous $PbCl_2$-OLA suspension under magnetic stirring. Sulfur (10.7 g, 0.33 mMol, Sigma-Aldrich, 100%) was first dissolved thoroughly in OLA (2.5 mL) at room temperature. The sulfur solution was degassed by purging N_2 gas and heated to 90 °C and then quickly injected into the $PbCl_2$-OLA suspension under vigorous stirring. The reaction was kept at the same temperature for 6 min, getting the monodispersed PbS QDs (size: ≈5 nm). The reaction mixture were taken from the reaction flask and quenched into cold hexane. Purification of PbS QDs was conducted with ethanol to completely remove the un-reacted precursors by repeated centrifugation and decantation.

2.2 Functionalization of MWCNTs and their subsequent hybridization with PbS-QDs

MWCNTs (Nanolab, Brighton, MA) were dispersed in 3 M HNO_3 solution under sonication for four hours at room temperature. This treatment was to form carboxylic acid groups on CNT surface. The acid treated MWCNTs were washed with distilled water until the pH value was close to 7. After complete drying at 80 °C, the MWCNTs were dispersed in toluene via sonication. Then, a certain amount of OLA was added to the toluene solution of MWCNTs with alternate cycles of sonication and vibration for 20 min. Then, different amounts of OLA-capped PbS QDs (dispersed in toluene) were mixed with OLA-modified MWCNTs in toluene by sonication for 5 min and vibration for 10 min. After purification via centrifugation and discarding the supernatant to remove those unattached free QDs, the obtained QD-decorated MWCNT hybrids were either directly used for characterization and evaluation or mixed with polymers to form polymeric nanohybrids. Only photoluminescence (PL) measurements were performed on un-purified hybrid samples, which contain some free QDs.

2.3 TEM and transient absorption measurements

Morphology and microstructure of PbS-QDs, MWCNTs and their nano-architecture were characterized by a field emission high-resolution transmission electron microscope (HRTEM, JEOL JEM-2100F). Optical properties were performed on thin films of PbS-QDs, (PbS QDs + MWCNTs) and (PbS QDs + MWCNTs + polymers) prepared using drop casting or spin coating. Absorption spectra of thin films were taken on a UV-vis-NIR spectrometer (Cary 5000, Varian). Steady state and dynamic PL was measured using an excitation wavelength of 670 nm and a 636 nm diode laser, respectively, on a Fluorolog – 3 spectrofluorometer (Horiba Jobin Yvon). All experiments were carried out under ambient conditions.

2.4 Fabrication of photovoltaic cells

In this study, we have fabricated four different types of PV cells. The first type of device is known as the controlled standard solar cell, whereas the second, third, and fourth type of photovoltaic (PV) cells are known as hybrid device – I, – II and – III, respectively. These PV cells were fabricated by spin-coating different recipe of photoactive nanocomposites such as; P3HT:PCBM, (P3HT:PCBM):PbS-QD/MWCNT, (P3HT:PCBM):PbS-QD and P3HT:PbS-QD:MWCNT, respectively. The individual spin coated photoactive layers were sandwiched between two electrodes, i.e., one made of indium-tin-oxide (ITO) as (semi-)transparent and conducting anode, whereas the other one is made of lithium fluoride (LiF)/aluminum (Al) as reflective and low-work function cathode. The ITO pre-coated glass was first lithography patterned by and etching according to the desired device geometric configuration. The patterned glass/ITO substrates were thoroughly cleaned by subsequent ultrasonic bath for 20 min each in acetone, isopropyl alcohol (IPA) and de-ionized water (DI-H_2O). The patterned and cleaned ITO was covered by spin-coating with a 40 nm thick layer of poly(3,4-ethylenedioxythiophene) doped with highly conducting electronic grade poly(styrenesulfonate) (PEDOT:PSS, Clevios^{TM} P VP Al 4083 from H.C. Starck), then baked at 120 °C for ∼1 h in ambient air before being transferred to a nitrogen-filled glove box (mBRAUN) for the photoactive layer deposition.

The as-synthesized PbS-QD/MWCNT was dispersed in toluene (40 mg/mL for PbS QDs; 1.0 mg/mL for MWCNTs) and then was further incorporated into the nanoblend of regioregular poly(3-hexylthiophene) (rr-P3HT) (Rieke Metals, Inc.) and phenyl-C_{61}-butyric acid methyl ester (PCBM) (Sigma-Aldrich) according to the following procedures. The P3HT andPCBM were separately dissolved in common organic solvent anhydrous 1, 2-dichlorobenzene (DCB) with concentrations of 10 mg/mL and 8 mg/mL, respectively. The two individual solutions were stirred at 50 °C for ∼1 h inside the glove box, and then mixed together at a 1:0.8 wt/wt ratio. Prior to spin-coating, the P3HT:PCBM solution was stirred at 40 °C for ∼16 h inside the glove box. For the nanohybrid device – I, the standard P3HT:PCBM solution was mixed with a solution of nanohybridized PbS-QD/MWCNT at a vol/vol ratio of 2:1. For the nanohybrid device – II, the standard P3HT:PCBM solution and a PbS-QDs solution were mixed together at a vol/vol ratio of 2:1. Finally, for the non-hybridized device, a ternary blend of P3HT, PbS-QDs and MWCNTs were physically mixed together at a ratio of 2:1:1 (in volume). All the four solutions were then stirred at 40 °C for ∼1 h inside the glove box. Each final blend was spin-coated at 1000 rpm for 60 s onto the patterned glass/ITO/PEDOT:PSS substrates, then transferred to petri-dishes and left to dry for about ∼1 h. The samples were then baked at 140 °C for ∼1 h prior to the cathode deposition. In order to proceed to the cathode deposition, the samples were moved from the glove box to the evaporation chamber. During this transfer, the spin-coated photoactive layers were exposed to the general ambient air. A 1.0 nm thick lithium fluoride (LiF) was used as the interfacial layer, and then followed by the deposition of a 100 nm thick top aluminum (Al) electrode without breaking the vacuum of $\sim 1 \times 10^{-6}$ mbar. The deposition rates of the various materials were calibrated by Dektak profilometer measurements then monitored by quartz microbalance during deposition. The active area of the devices was 0.2 cm^2.

2.5 Characterization of photovoltaic cells:

The solar cell PCE characterization was carried out in air by using a solar simulator made from a 150 W Oriel Xenon-lamp equipped with an AM1.5G filter (at an intensity of 100 mW cm^{-2}). The current-voltage (*I-V*) characterization of the PV cells were performed by using a Keithley 2400 programmable voltage source meter. Wavelength resolved measurements were carried out by using an Oriel monochromator. The cells were characterized upon probing with different wavelengths ranging from 400 nm to 1800 nm to determine the short-circuit current density (J_{sc}) and open-circuit voltage (V_{oc}). In all device cases, the measurements were performed from a set of at least 16 PV cells and the reported short-circuit current density (J_{sc}), open-circuit voltage (V_{oc}), fill factor (FF), and power conversion efficiency (PCE) values were taken as the average from those sets of measurements.

3 Results and discussion

First, we fabricate our controlled standard OPV cell from a nanocomposite of P3HT:PCBM nanocomposites active layer in order to set a standard of power conversion efficiency (PCE) under the standard experimental conditions in our laboratory (materials, air exposure, measurement conditions, etc.) [31–33]. The measured photocurrent density (*J*) as a function of applied voltage (*V*) of the standard PV cell, illuminated under AM1.5G solar spectrum at intensity of 100 mW cm^{-2}, is shown in Figure 1. The short-circuit current density (J_{sc}), open-circuit voltage (V_{oc}) and fill factor (FF) of this control device were measured to be 8.82 mA/cm^2, 0.54 V and 54%, respectively, as enlisted in Table 1. Power conversion efficiency (PCE) of 2.57% was evaluated from these measurements which is an appropriate value for PV cells fabricated and characterized upon air exposure and also comparable with our previously reported results [31,33]. Next, we fabricate the hybrid device – I upon merely adding hybridized PbS-QD/MWCNTs into the standard polymer/fullerene (P3HT:PCBM) blend. The *J-V* characteristics of hybrid device – I are shown in Figure 1. This hybrid device – I (versus the standard P3HT:PCBM device) exhibited an increase in power conversion efficiency up to 3.40% which is mainly attributed to the increase in J_{sc} up to 12.12 mA/cm^2, without any significant change in V_{oc}. The summarized key parameters were determined from the *J-V* characteristic curves and enlisted in Table 1.

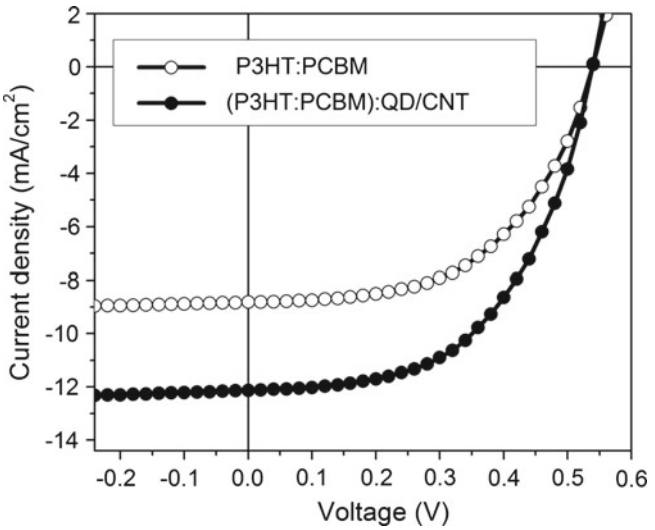

Fig. 1. The open black circles and filled black spheres represent the current density-voltage (*J-V*) characteristics of the standard P3HT:PCBM and nanohybrid (P3HT:PCBM):QD/CNT based PV cells, respectively, are simulated under AM1.5G spectrum of intensity 100 mW cm^{-2}.

Table 1. Key parameters were determined from *J-V* characteristic curves obtained from PV cells.

Type of PV cells	J_{sc} (mA/cm^2)	V_{oc} (V)	FF (%)	PCE (%)
P3HT:PCBM	8.82	0.54	54	2.57
(P3HT:PCBM):QD/CNT	12.12	0.54	52	3.40
(P3HT:PCBM):QD	9.49	0.54	55	2.82
P3HT:QD:CNT	2.28	0.52	47	0.56

In order to explore the mechanism(s) that govern the increased PCE of the organic/inorganic hybrid PV cell, we have performed the wavelength resolved short circuit current density (J_{sc}) and open circuit voltage (V_{oc}) measurements, shown in Figures 2a, and 2b, respectively. Upon probing the standard P3HT:PCBM PV cell at different wavelengths, a measurable J_{sc} was consistently observed for the probed wavelengths between 400 nm and 650 nm. However, the J_{sc} starts to decrease beyond 650 nm, and it is almost nil beyond 750 nm. For the (P3HT:PCBM):PbS-QD/MWCNT hybrid device – I, the J_{sc} was consistently measured over wavelengths ranging from 400 nm to 1450 nm. However, beyond 1450 nm, J_{sc} value drastically decreases and is nil beyond 1700 nm. It is then clearly seen from the Figure 2a that the J_{sc} values measured for wavelength between 650 nm to 1450 nm in hybrid device – I should be due to charges generated in the presence of quantum-dot-sensitized PbS [31]. In Figure 2b, the wavelength resolved open circuit voltage (V_{oc}) measurements were carried out on those same standard and hybrid devices at different wavelengths, similar effect for V_{oc} was observed as it was observed for J_{sc} in Figure 2a. The V_{oc} values were observed consistently upon probing the hybrid device – I at the wavelength between 400 nm to 1450 nm, whereas the standard device exhibits the V_{oc} output limited to a certain probed wavelength of 400 nm to 650 nm. Therefore, it can be justified that the presence of PbS-QDs, in hybrid device – I, extends the spectral sensitivity towards the NIR regime for the light harvesting, which further contributes to the effective enhancement in PCE [31]. This wavelength resolved measurements are consistent with our previously reported absorption measurements from UV/vis through NIR of the spectral regime for the hybrid photoactive films [31].

In order to further quantify the potential role of PbS-QDs and/or MWCNTs in the hybrid devices, we have fabricated another controlled device, upon adding a mere amount of PbS-QDs into the standard P3HT:PCBM nanocomposite, known as hybrid device – II. The *J-V* characteristic curve of this (P3HT:PCBM):PbS based hybrid device – II has shown in Figure 3. This hybrid device – II (without MWCNT hybridization) exhibits a PCE of 2.82%, which is about ca. 21% lower in efficiency than that of the (P3HT:PCBM):QD/CNT based hybrid device – I, as compared in Table 1. In this experiment, the device without MWCNTs demonstrates the important role

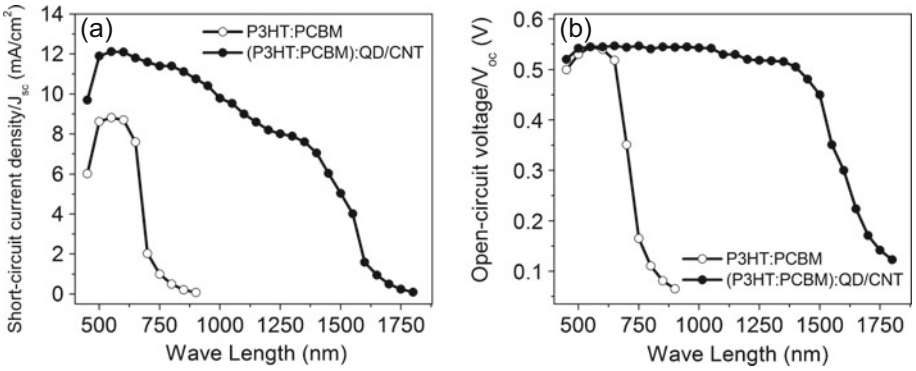

Fig. 2. Wavelength resolved (a) short-circuit current density (J_{sc}), and (b) open-circuit voltage (V_{oc}) of the (P3HT:PCBM)PbS-QD/MWCNT nanohybrid based device in comparison with the standard P3HT:PCBM device measured under the spectrum influx of monochromatic wavelength between 450 nm and 1800 nm. Please note that while the light intensity at each wavelength could not be measured exactly, these qualitative results have clearly shown that the device is appropriately responding to NIR light when containing PbS-QD/MWCNT [31].

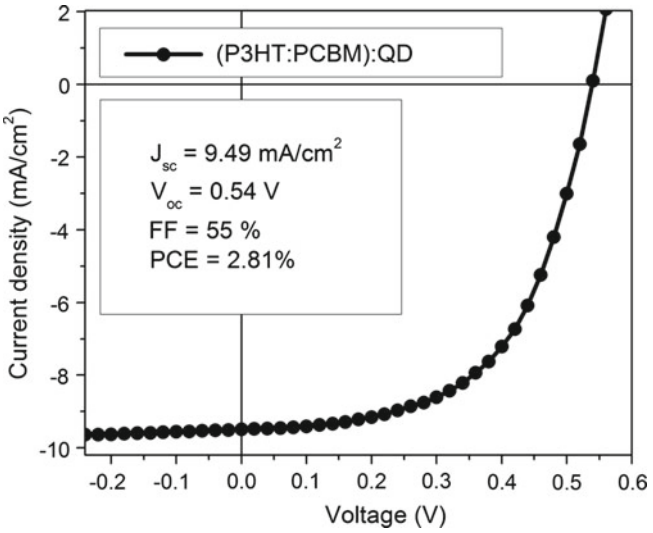

Fig. 3. The filled black spheres represent the *J-V* characteristics, and the inset text shows the J_{sc}, V_{oc}, FF and PCE of the (P3HT:PCBM):PbS based PV cell, simulated under AM1.5G spectrum of intensity 100 mW cm^{-2}.

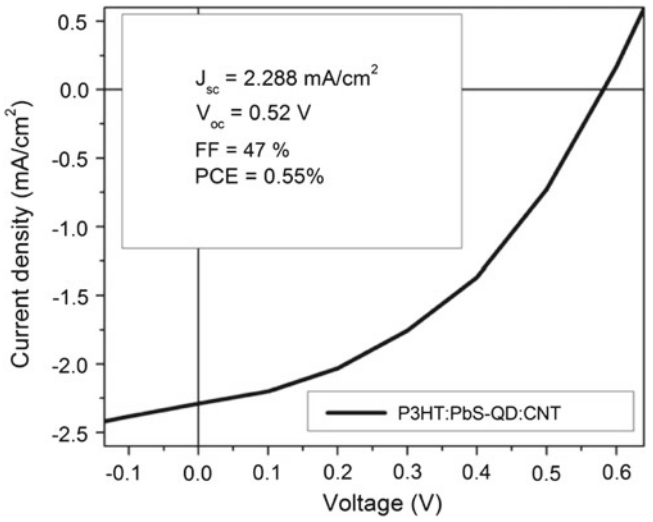

Fig. 4. The curves represent the *J-V* characteristics, and the inset text shows the J_{sc}, V_{oc}, FF and PCE of the P3HT:PbS:MWCNT based PV cell, simulated under AM1.5G spectrum of intensity 100 mW cm^{-2}.

of CNTs governing the enhancement of PCE which is attributed to the increase in J_{sc} of the nanohybrid structured solar cells.

In order to demonstrate the importance of strong conjugation of PbS-QDs in close proximity with the MWCNTs, an additional experiment was conducted. For such a strategic experiment, we have fabricated a typical device from a simple physical mixture of P3HT:PbS:MWCNT blend, i.e., a ternary blend of P3HT, PbS-QDs, and MWCNTs (without any hybridization of PbS-QDs to the MWCNTs). The *J-V* characteristic curve of P3HT:PbS:MWCNT hybrid device – III is shown in Figure 4. The efficiency of this device is as low as 0.56% and is

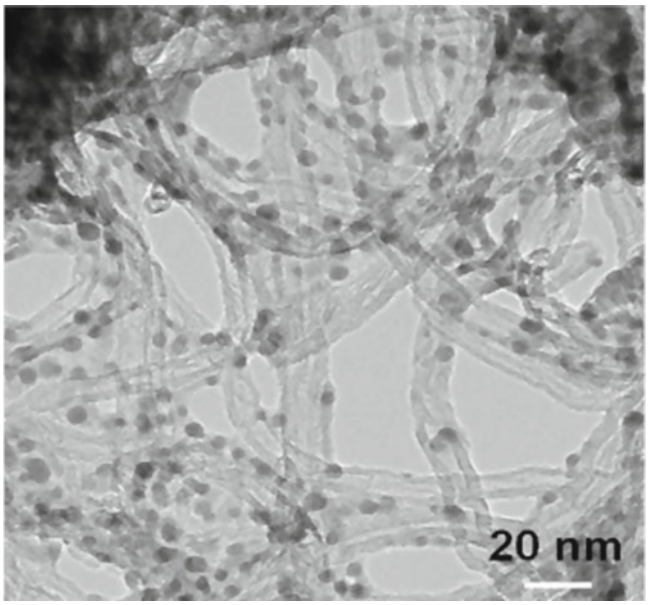

Fig. 5. TEM images of the nanohybrids PbS-QDs/MWCNTs showing coverage of PbS-QDs on the MWCNT surfaces.

attributed to the modest J_{sc} which is several order lower in magnitude than that of the hybridized P3HT:PbS/MWCNT as reported earlier in one of our previous communication [31]. In principle, P3HT:PbS is referred to as a "hole-transport only" system [14]. Therefore, this modest charge transport across the bulk of the photoactive layer and moderate photo-exciton dissociation at the donor/acceptor interface hinders the efficiency of PV cells. This experiment suggests the importance of controlled and strong conjugation between PbS-QDs and MWCNTs.

Although the role of PbS-QDs in the hybrid photoactive films seems to be well explained by their properties of extending the spectral sensitivity to harvest the light in NIR regime, the role of CNTs in the hybrid films still has to be further clarified. CNTs can be a direct path of charge transport to the electrode and can be used as the electron acceptor [34,35]. This observation also explains the CNTs substitute in place of PCBM and serves efficiently as electron transport through ballistic pathways instead of by slow hopping and tunnelling among phase separated clusters as the case for QD – only devices [26–30]. Therefore, an enhancement in J_{sc}, and as a result an improved PCE, is observed in the devices comprised of nanohybridized QD/CNT based photoactive layer. In Figure 5, a typical TEM image shows the strong and stable interaction between the QD attached to and MWCNT surfaces in close proximity with each other. Therefore, the photo-generated carriers formed by QDs are further being efficiently transported to the covalently bonded functionalized MWCNTs, suggesting a fast charge transfer between QDs and CNTs [36]. Aiming to understand the mechanism(s) of the controlled coupling and interaction between PbS-QDs and MWCNTs and their respective transportation of photo-generated carriers, an effort was taken to perform absorption measurements on the PbS-QD/MWCNT nanoarchitecture films. Figure 6

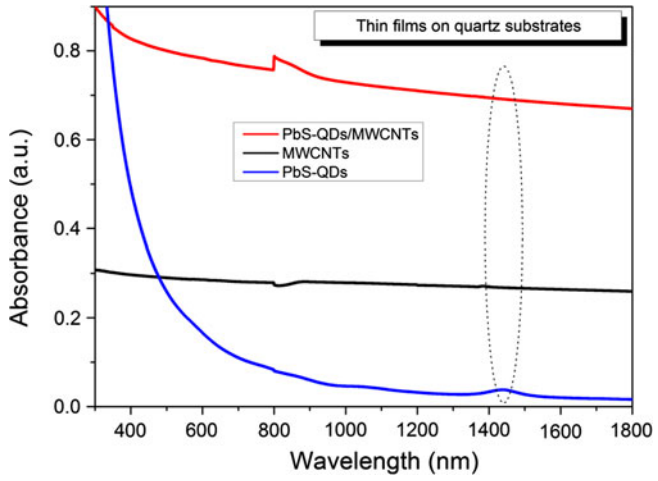

Fig. 6. Absorption spectra of the PbS-QD film, MWCNT film and PbS-QD/MWCNT nanohybrid films. The ratio of the components in the nanohybrids were determined by absorption measurement of the original PbS-QDs and the supernatant after purification of the PbS-QD/MWCNT nanoarchitecture. The weight ratio of PbS-QDs/MWCNTs in the PbS-QD/MWCNT nanoarchitecture was 4:1. The thin film samples were prepared upon drop casting the solutions onto the quartz substrates.

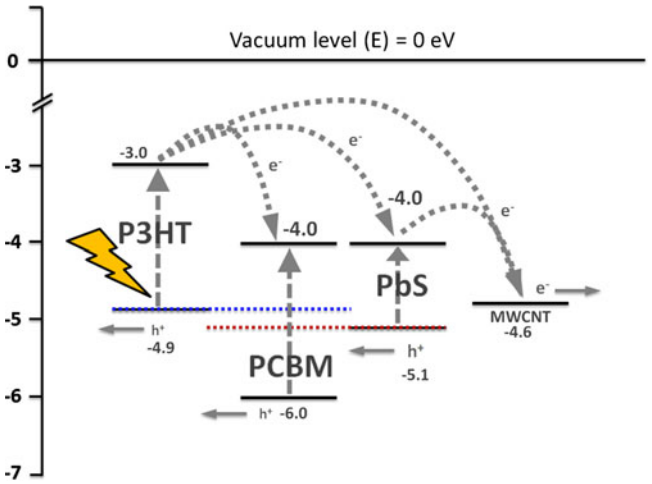

Fig. 7. The schematic illustration of a nanohybrid architecture (P3HT:PCBM):PbS/MWCNT PV cell demonstrating the working mechanism of exciton generation, subsequent exciton dissociation and followed by the carrier transport while under operational at UV/Vis through the NIR region of the spectrum. Hole and electron transports are represented by arrows. Energy band diagram displaying HOMO and LUMO of polymer donor-acceptor materials, as well as the valence and conduction band edge of inorganic PbS-QD acceptor. Values were taken from the references [1,14,28,31,33,37,38].

shows the absorption spectra of PbS-QD, MWCNT, and PbS-QD/MWCNT nanohybrid films. From the absorption spectrum of MWCNTs, it is clearly indicate that the MWCNTs do not show any characteristic absorption peak but basically a constant absorbance value throughout the wavelength range investigated herein. However, in the spectrum of PbS-QD/MWCNT nanoarchitecture, the absorbance shows a gradual increase similar to that of pure PbS-QDs towards shorter wavelength range, indicating the contribution of PbS-QDs. However, the characteristic exciton absorption peak (∼1450 nm) of PbS-QDs eventually vanished in the QD/CNT nanoarchitecture, suggesting the strong interaction and controlled coupling between PbS-QDs and MWCNTs irrespective of the presence of long-chain OLA molecules [30,31,35]. Nevertheless, it is clear that the absorption of PbS-QD/MWCNT nanohybrids extended deep into the near infrared (NIR) wavelength regime which is mainly attributed to the presence of PbS-QDs. As a result, the enhanced PV performance was obtained from the (P3HT:PCBM):PbS-QD/MWCNT nanohybrid based PV cells.

It is of paramount importance to address the working principle of the PV cells in all these prolonged absorption range (i.e., from 450 nm to 1450 nm) of the incident solar spectrum for a hybrid PV system. A schematic illustration is depicted in Figure 7, with all the photoactive materials used in this experiment along with their respective energy levels [1,14,28,31,33,37,38], in order to explain the working mechanism(s). In a ternary nanoblend of (P3HT:PCBM):PbS/MWCNT, it has been reported that there is almost a flat band condition between the LUMO of PCBM and the conduction band of PbS-QDs [14,39] as shown in Figure 7. Therefore, the enhanced photocurrent is finally yielded in the external circuit without any change in V_{oc} due to the staggered favorable energy band-alignment between P3HT and the QDs allows both electron and hole transfer from the QDs to the PCBM and the P3HT, respectively [14]. The excitons generated in the PbS-QDs can efficiently dissociate at the QD/CNT interface and injected electrons can be further transported by the CNTs to either of the favorable electrodes in the hybrid systems. This also explains the important contribution of CNTs towards the improvement of PV performances. On the other hand, the P3HT:PbS/MWCNT device, with hybridization of PbS-QDs to the MWCNTs, provide a direct and efficient channel-pathway for the transport of conduction-band electrons to the cathode [40]. The remaining holes in the QDs may move towards the anode [41], via HOMO of P3HT, is being supported by the favorable energy band alignment between P3HT and the QDs [14]. The process of working principle of this (P3HT:PCBM):PbS/MWCNT PV cell is shown in Figure 7. Therefore, the (P3HT:PCBM):PbS/MWCNT device shown to be the best PV cell among other four PV cells. The efficiency of this (P3HT:PCBM):PbS/MWCNT PV cell is observed to be ∼ 32% larger than that of the standard P3HT:PCBM PV cell.

Based on the above experimental results, it can be suggested that in our (P3HT:PCBM):QD/CNT based hybrid device, an important aspect is the use of PbS-QDs in the hybrid films for enhancing the extended spectral sensitivity from visible through the NIR regime of the spectrum. The other main feature is; the semiconducting PbS colloidal QDs (in the QD/MWCNT nanohybrids) served as donors for the electron-accepting PCBMs. The charge

transport was also further efficiently assisted by the presence of CNTs due to their dual electronic nature since the CNTs can either be preferentially employed as a donor – or acceptor – type materials [34,35]. This is consistent with the band diagram shown in Figure 7 and with aid of this band diagram we able to explain that the excitons generated in PbS-QDs in the NIR region, can be dissociated at the PbS/MWCNT interface to yield photocurrent in the external circuit. This is also explained with the consistently observed V_{oc} for all the samples.

Until now, it has been long-debated in literature to address the exact mechanism for the origin of V_{oc} in photovoltaics and has been still under investigation [42–47]. However, it can be quantified by the energy difference between the lowest unoccupied molecular orbital (LUMO) of the acceptor – and the highest occupied molecular orbital (HOMO) of the donor – type materials at the heterojunction interface [42–44,46,47]. We explain the charge transport mechanism(s) behind the consistently observed V_{oc} in all our devices with the aid of energy band diagram shown in Figure 7. The energy level values were taken from the references elsewhere [1,14,28,31,33,37,38]. In all our devices, the P3HT was used as donor with respect to the PCBM and/or nanohybrid of QD/CNT as the acceptor(s). We presume that the V_{oc} can be attributed to the energy difference between the HOMO of P3HT and LUMO of PCBM in our standard cell as it has been reported by other research groups [42–47]. Since the value of conduction band of PbS-QDs is consistently aligned with the LUMO value of PCBM [1,14,28] as shown in Figure 7, therefore it is obvious that the V_{oc} of hybrid device – I is consistent with the standard P3HT:PCBM devices. This explains the charge transfer takes place at P3HT/PCBM interface in the case of standard devices, whereas the same phenomenon of charge transfer occurs at the interface(s) of P3HT/PbS and/or P3HT/(PCBM/PbS) in case of the hybrid devices.

4 Conclusion

In summary, we devised an alternative nanohybrid-architecture-approach for solar cells to improve performance upon loading the controlled hybridization of PbS-QD/MWCNT into the standard P3HT:PCBM nanocomposite. The modified (P3HT:PCBM):PbS-QD/MWCNT BHJ shown an increased PCE of 3.40% which is ca. 32% significantly larger than that of the standard P3HT:PCBM BHJ PV cell. The improved efficiency is mainly due to the enhancement in J_{sc}, which is attributed to the extended spectral sensitivity for the NIR (absorption between ∼700 nm to ∼1450 nm) photon-to-electron conversion. Upon incorporating QD/CNTs nanohybrid structures, the charge-injection steps were effectively improved by the potential aid of CNTs. This causes the holes extraction from the excited states of P3HT to further generate the charge separation states. The enhancement in J_{sc} results in the hybrid cells is further supported by the wavelength resolved efficiency characterization. The V_{oc} values are observed to be unchanged in all the PV cells, since it can be argued that the charge transfer occurs at the P3HT/PCBM interface in the case of a standard cell, whereas the same phenomenon of charge transfer occurs at the interface of P3HT/PbS and/or P3HT/(PCBM/PbS) interfaces in the case of organic/inorganic hybrid devices. Therefore, our alternative approach of incorporating the nanohybrids of NIR-sensitized QD/CNTs into the standard polymer/fullerene could be applicable to other similar systems to enhance the photovoltaic effects.

We thank the Natural Science and Engineering Research Council of Canada (NSERC), the "Centre Québécois sur les Matériaux Fonctionnels" (CQMF), the "Fonds Québécois de Recherche sur la Nature et les Technologies" (FQRNT) and Sixtron advanced Materials, in the context of a CRD-NSERC Grant (CRDPJ 379634 – 08) are acknowledged for the financial support to carry out this research work.

References

1. K.M. Noone, E. Strein, N.C. Anderson, P.-T. Wu, S.A. Jenekhe, D.S. Ginger, Nano Lett. **10**, 2635 (2010)
2. H. Hoppe, N.S. Sariciftci, J. Mater. Res. **19**, 1924 (2004)
3. H.J. Snaith, A.J. Moule, C. Klein, K. Meerholz, R.H. Friend, M. Gratzel, Nano Lett. **7**, 3372 (2007)
4. L. Schmidt-Mende, U. Bach, R.H. Baker, T. Horiuchi, H. Miura, S. Ito, S. Uchida, M. Gratzel, Adv. Mater. **17**, 813 (2005)
5. W.U. Huynh, J.J. Dittmer, A.P. Alivisatos, Science **295**, 2425 (2002)
6. S.D. Oosterhout, M.M. Wienk, S.S. van Bavel, R. Thiedmann, L.J.A. Koster, J. Gilot, J. Loos, V. Schmidt, R.A.J. Janssen, Nat. Mater. **8**, 818 (2009)
7. G. Dennler, M.C. Scharber, C.J. Brabec, Adv. Mater. **21**, 1323 (2009)
8. M.M. Wienk, J.M. Kroon, W.J.H. Verhees, J. Knol, J.C. Hummelen, P.A. van Hal, R.A.J. Janssen, Ang. Chem. Int. Ed. **42**, 3371 (2003)
9. Y. Liang, Z. Xu, J. Xia, S.-T. Tsai, Y. Wu, G. Li, C. Ray, L. Yu, Adv. Mater. **22**, E135 (2010)
10. M. Wright, A. Uddin, Sol. Energy Mater. Sol. Cells **107**, 087 (2012)
11. M.A. Green, K. Emery, Y. Hishikawa, W. Warta, E.D. Dunlop, Prog. Photovolt. Res. Appl. **20**, 12 (2012)
12. T. Ameri, N. Li, C.J. Brabec, Energ. Environ. Sci. **6**, 2390 (2013)
13. J.Y. Kim, K. Lee, N.E. Coates, D. Moses, T.-Q. Nguyen, M. Dante, A.J. Heeger, Science **317**, 222 (2007)
14. T. Rauch, M. Böberl, S.F. Tedde, J. Fürst, M.V. Kovalenko, G. Hesser, U. Lemmer, W. Heiss, O. Hayden, Nature Photonics **3**, 332 (2009)
15. A.P. Alivisatos, Science **271**, 933 (1996)
16. C.B. Murray, D.J. Norris, M.G. Bawendi, J. Am. Chem. Soc. **115**, 8706 (1993)
17. B.O. Dabbousi, J. Rodriguez-Viejo, F.V. Mikulec, J.R. Heine, H. Mattoussi, R. Ober, K.F. Jensen, M.G. Bawendi, J. Phys. Chem. B **101**, 9463 (1997)
18. J. Tang, J. Brzozowski, D.A.R. Barkhouse, X. Wang, R. Debnath, R. Wolowiec, E. Palmiano, L. Levina, A.G. Pattantyus-Abraham, D. Jamakosmanovic, E.H. Sargent, ACS Nano **4**, 869 (2010)

19. R.J. Ellingson, M.C. Beard, J.C. Johnson, P. Yu, O.I. Micic, A.J. Nozik, A. Shabaev, A.L. Efros, Nano Lett. **5**, 865 (2005)
20. R.D. Schaller, M. Sykora, J.M. Pietryga, V.I. Klimov, Nano Lett. **6**, 424 (2006)
21. J.M. Luther, M. Law, M.C. Beard, Q. Song, M.O. Reese, R.J. Ellingson, A.J. Nozik, Nano Lett. **8**, 3488 (2008)
22. D.A.R. Barkhouse, A.G. Pattantyus-Abraham, L. Levina, E.H. Sargent, ACS Nano **2**, 2356 (2008)
23. K.W. Johnston, A.G. Pattantyus-Abraham, J.P. Clifford, S.H. Myrskog, D.D. MacNeil, L. Levina, E.H. Sargent, Appl. Phys. Lett. **92**, 151115 (2008)
24. G.I. Koleilat, L. Levina, H. Shukla, S.H. Myrskog, S. Hinds, A.G. Pattantyus-Abraham, E.H. Sargent, ACS Nano **2**, 833 (2008)
25. A. Guchhait, A.K. Rath, A.J. Pal, Appl. Phys. Lett. **96**, 073505 (2010)
26. E. Kymakis, G.A.J. Amaratunga, Appl. Phys. Lett. **80**, 112 (2002)
27. S. Berson, R. de Bettignies, S. Bailly, S. Guillerez, B. Jousselme, Adv. Funct. Mater. **17**, 3363 (2007)
28. M.-C. Wu, Y.-Y. Lin, S. Chen, H.-C. Liao, Y.-J. Wu, C.-W. Chen, Y.-F. Chen, W.-F. Su, Chem. Phys. Lett. **468**, 64 (2009)
29. L. Liu, W.E. Stanchina, G. Li, Appl. Phys. Lett. **94**, 233309 (2009)
30. D.M. Guldi, G.M.A. Rahman, F. Zerbetto, M. Prato, Acc. Chem. Res. **38**, 871 (2005)
31. D. Wang, J.K. Baral, H. Zhao, B.A. Gonfa, V.-V. Truong, M.A.E. Khakani, R. Izquierdo, D. Ma, Adv. Funct. Mater. **21**, 4010 (2011)
32. H. Zhao, M. Chaker, D. Ma, J. Phys. Chem. C **113**, 6497 (2009)
33. J.K. Baral, R. Izquierdo, M. Packirisamy, V.-V. Truong, Eur. Phys. J. Appl. Phys. **55**, 30202 (2011)
34. J. Geng, B.-S. Kong, S.B. Yang, S.C. Youn, S. Park, T. Joo, H.-T. Jung, Adv. Funct. Mater. **18**, 2659 (2008)
35. V. Sgobba, D.M. Guldi, J. Mater. Chem. **18**, 153 (2008)
36. S. Azoz, J. Jiang, G. Keskar, C. McEnally, A. Alkas, F. Ren, N. Marinkovic, G.L. Haller, S. Ismail-Beigi, L.D. Pfefferle, Nanoscale **5**, 6893 (2013)
37. B. Pradhan, S.K. Batabyal, A.J. Pal, Appl. Phys. Lett. **88**, 093106 (2006)
38. H. Ago, T. Kugler, F. Cacialli, W.R. Salaneck, M.S.P. Shaffer, A.H. Windle, R.H. Friend, J. Phys. Chem. B **103**, 8116 (1999)
39. N. Zhao, T.P. Osedach, L.-Y. Chang, S.M. Geyer, D. Wanger, M.T. Binda, A.C. Arango, M.G. Bawendi, V. Bulovic, ACS Nano **4**, 3743 (2010)
40. F. Li, S.H. Cho, D.I. Son, T.W. Kim, S.-K. Lee, Y.-H. Cho, S. Jin, Appl. Phys. Lett. **94**, 111906 (2009)
41. M. Nam, S. Kim, T. Kim, S.-W. Kim, K.-K. Lee, Appl. Phys. Lett. **99**, 233115 (2011)
42. C.J. Brabec, A. Cravino, D. Meissner, N.S. Sariciftci, T. Fromherz, M.T. Rispens, L. Sanchez, J.C. Hummelen, Adv. Funct. Mater. **11**, 374 (2001)
43. M.C. Scharber, D. Mühlbacher, M. Koppe, P. Denk, C. Waldauf, A.J. Heeger, C.J. Brabec, Adv. Mater. **18**, 789 (2006)
44. W.J. Potscavage Jr., S. Yoo, B. Kippelen, Appl. Phys. Lett. **93**, 193308 (2008)
45. S.E. Gledhill, B. Scott, B.A. Gregg, J. Mater. Res. **20**, 3167 (2005)
46. A. Gadisa, M. Svensson, M.R. Andersson, O. Inganäs, Appl. Phys. Lett. **84**, 1609 (2004)
47. K.L. Mutolo, E.I. Mayo, B.P. Rand, S.R. Forrest, M.E. Thompson, J. Am. Chem. Soc. **128**, 8108 (2006)